ELSEVIER

Infrared Physics & Technology 42 (2001) 189–198

INFRARED PHYSICS & TECHNOLOGY

www.elsevier.com/locate/infrared

Microstrip antenna coupling for quantum-well infrared photodetectors

William A. Beck [a,*], Mark S. Mirotznik [b]

[a] US Army Research Laboratory, AMSRL-SE-EI, 2800 Powder Mill Road, Adelphi, MD 20783, USA
[b] The Catholic University of America, Washington, DC, USA

Abstract

We computed the expected performance of microstrip antennas as optical couplers in quantum-well infrared photodetectors (QWIPs) by the finite-difference time-domain technique. The microstrip antenna consisted of a metal square that is placed on one side of a thin QW stack, across from a continuous ground plane on the other side of the stack. The size of the square was one-half wavelength in the QW material, or ~1.2 μm for a long-wavelength GaAs/AlGaAs QWIP. An array of these antennas can be used to couple to an arbitrary-size pixel. Unlike the elements of a diffraction grating, each antenna in the array acts as a nearly independent coupler whose peak wavelength is determined by the dimensions of the antenna, not by the period of the antenna array. Because of this local coupling, the array of microstrip antennas maintains absorption in small pixels much more effectively than do grating couplers. Furthermore, the microstrip antenna yields moderately high absorption over a useful spectral bandwidth with a very thin QW stack. Such a stack has a high photoconductive gain, which is useful for many applications.

PACS: 85.60 Gz; 85.30 De; 84.40 Ba

Keywords: Quantum-well infrared photoconductor; Infrared detector; Antenna; Coupling

1. Introduction

Most current quantum-well infrared photodetectors (QWIPs) use a periodic metal diffraction grating to facilitate absorption of normally incident light [1–4]. The grating, or an alternative optical coupling structure, is required because the absorption cross-section for light propagating through the QWs is $\sigma = \sigma_0(\hat{\mathbf{E}} \cdot \hat{\mathbf{n}})^2$, where σ_0 is the absorption cross-section for light propagating tangential to the QWs with the electric field oriented perpendicular to the QWs, $\hat{\mathbf{E}}$ is the electric field polarization vector, and $\hat{\mathbf{n}}$ is a unit vector perpendicular to the QWs. An efficient coupling structure diffracts most of the normally incident light (with $\hat{\mathbf{E}} \cdot \hat{\mathbf{n}} = 0$) into modes with $\hat{\mathbf{E}} \cdot \hat{\mathbf{n}} \approx 1$. To be useful in focal plane arrays (FPAs), the coupling structure must also work in relatively small pixels that are only two or three wavelengths wide.

Current grating-coupled QWIPs achieve an absorption quantum efficiency (QE) of around 20 to 40%. This is adequate for many applications, especially those that are background limited. However, a QE higher than 50% would be useful for

* Corresponding author. Tel.: +1-301-394-2085; fax: +1-301-394-5270.
E-mail address: wbeck@arl.army.mil (W.A. Beck).

1350-4495/01/$ - see front matter
PII: S1350-4495(01)00076-7

other applications that require a fast frame rate or a high *f*-number. Furthermore, the coupling efficiency of grating-coupled QWIPs tends to decrease in smaller pixels. This occurs for two reasons: (1) the number of periods in the diffraction grating decreases with pixel size, and (2) the diffracted modes that interact with the quantum-well stack are *extended* modes that propagate across the full width of the pixel. These extended modes interact with the sides of the pixel such that the coupling in a small pixel is a complex interaction between the pixel cavity modes and the grating modes. It would be useful to have a coupling method that scales to small pixels with minimal loss of efficiency.

Finally, gratings must be etched. A planar process would be somewhat lower in cost and eliminate variation in etch depth as a possible source of nonuniformity. These issues have stimulated interest in alternate coupling structures.

In addition to periodic metal diffraction gratings, QWIPs have been reported by others using pseudorandom [5,6] etched gratings, as well as periodic planar gratings [7]. These structures are also generally designed to couple via propagating modes above the grating. The pseudo-random grating scatters normally incident light into a wide range of angles, thereby avoiding coherent redifffraction out of the QWIP, and permitting more than two passes through the QW stack. In large pixels, a significant improvement of QE was observed with the pseudorandom over the periodic grating; however, the improvement decreases in smaller pixels [8].

Several groups have demonstrated designs in which the ''grating'' is etched through the QW stack either in a two-dimensional square lattice (the ''enhanced'' or EQWIP) [9] or as a set of parallel V-shaped grooves (the ''corrugated'' or C-QWIP) [10]. These designs depend less on propagating modes and more on localized modes, so that their performance is degraded much less in small pixels. The V-groove structure [10] also has a relatively wide spectral bandwidth.

Several workers have investigated coupling in infrared detectors by means of dipole antennas [11], bowtie antennas [12,13], log-periodic antennas [12], and spiral antennas [13–15]. In this paper, we investigate the use of microstrip antennas, which are appealing for QWIPs because they are planar and have demonstrated high efficiency at microwave frequencies [16]. Microstrip antennas have previously been demonstrated with infrared bolometers [17], although in a configuration that does not appear to be applicable for QWIPs. Therefore, we used rigorous three-dimensional electromagnetic modeling to predict the performance of several microstrip designs. The designs achieve QE similar to that obtained with gratings, but in much thinner structures, so that an increase in detectivity of almost a factor of three may be possible in dark-current-limited detectors. The antennas also provide a promising way to couple to single-QW structures grown for more basic research.

2. Approach

2.1. Microstrip antenna

Fig. 1a shows a typical microstrip antenna structure. It consists of a rectangular metal pad on one side of a dielectric slab and a continuous metal ground plane on the other side. In the usual microwave configuration, received energy is fed to microstrip transmission line that emerges at the center of one side of the antenna pad. The interaction of the antenna with the incident free-space radiation occurs primarily at the edges of the antenna pad, where incident radiation induces an electric field between the edge of the antenna pad and the ground plane directly below. The resonant wavelength of the antenna is determined by its length, i.e., by the dimension in the direction of the incident electric field. If a rectangular pad is used, the resonant wavelength is different for the two incident polarizations.

By placing a transmission line on both edges of the antenna (Fig. 1b), it is possible to achieve polarization-sensitive detection or, if the antenna is rectangular, two-colour detection with separate readouts. However, the use of these types of geometries for infrared wavelengths involves practical problems, to be discussed later. Therefore, we have concentrated on the simpler geometry shown in Fig. 2a, in which the QW stack is used as the

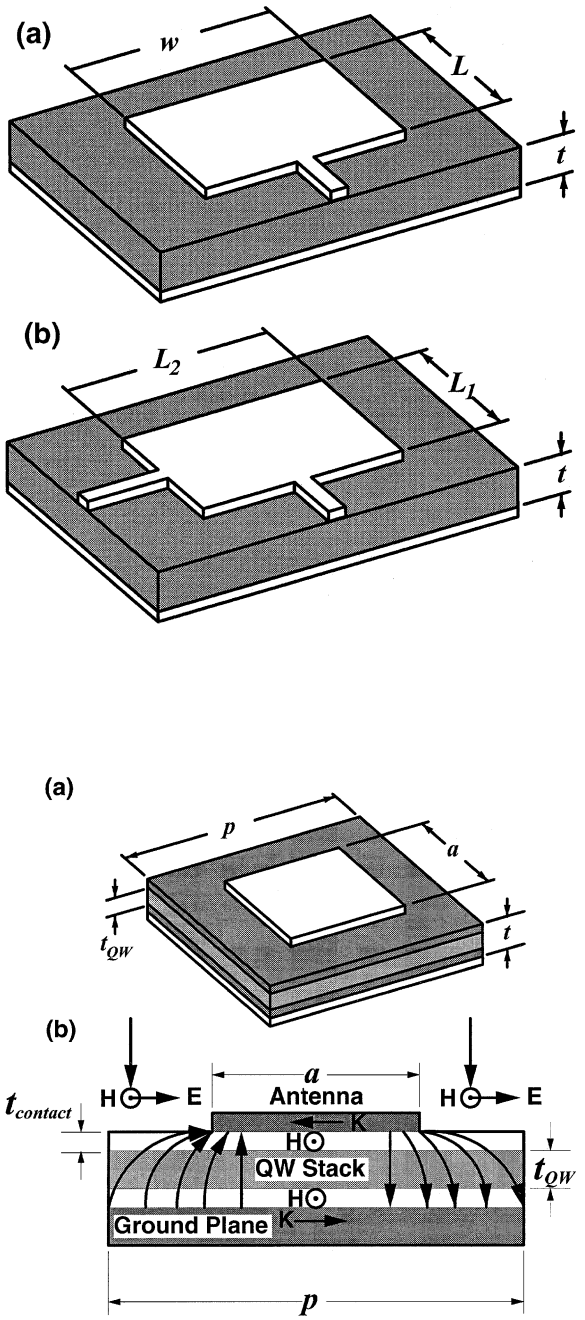

Fig. 2. Microstrip antenna-coupled QWIP unit cell. (a) Layout of square antenna and (b) cross-section showing electric (E) and magnetic (H) fields and surface currents (K).

dielectric slab, and absorption takes place directly under the antenna pad. As shown in Fig. 2b, the incident radiation excites the effective slots at each end of the pad, and thereby launches nearly transverse magnetic (TM) waves between the pad and ground plane that are at nearly the optimum direction and polarization for absorption by the QWs. A resonant standing wave is formed, and the strongest absorption occurs when the length of the antenna equals one-half wavelength in the dielectric slab (the QW stack). An array of antennas can be used to couple to an arbitrary-size pixel. Since the microstrip-antenna-coupled detector must be illuminated from the antenna side of the wafer, the antennas of a backside-illuminated FPA would be formed on the backside of the wafer after substrate thinning. This processing disadvantage offsets the advantage of eliminating the grating etch. However, the backside processing required to form the antennas is relatively simple.

Previous experimental [4] and computational [15] results show that finite conductivity of the metal used for the grating or antenna can significantly degrade QE. For example, earlier experiments [4] indicated that detectors with AuGe contacts had a QE that was 70% of the QE for detectors with pure gold contacts. The finite conductivity of even pure gold is significant, so the use of lower conductivity alloyed metals (used for ohmic contacts) should be minimized by the use of, for example, a hybrid contact with pure gold over most of the pixel area and alloys only near the edges of the pixel. As shown below, the microstrip antenna design is especially sensitive to the metal conductivity, so a similar hybrid contact would be advantageous.

2.2. Finite-difference time-domain method

A QWIP pixel is a somewhat challenging structure in which to compute electromagnetic coupling. The structure is inhomogeneous, including multiple layers of dielectrics and finite-conductivity metals. The QW stack itself is anisotropic. Finally, the structure has many potential resonances resulting from the periodicity of the optical coupler as well as from the pixel cavity itself.

The FDTD method [18,19] is well suited to solving problems of this type. The method is a

direct solution for Maxwell's time-dependent curl equations based on volumetric sampling of the unknown field distribution within and near the pixel over a period of time. The sampling in space is typically at 10–20 samples per wavelength (in the material). The sampling in time is selected to ensure numerical stability. For the results presented here, we first designed and gridded the QWIP pixel structures using a custom *Mathematica* notebook. We then ran the FDTD calculations using custom FDTD code written in FORTRAN90. Finally, we analyzed the results using custom software written in C++.

High- but finite-conductivity metals present a problem in FDTD (and other numerical electromagnetic techniques) because the fields change so rapidly near the surface of such a metal, thereby requiring an unreasonably small grid spacing to accurately describe the fields. For example, a grid spacing of 0.3 μm is acceptable in most sections of a QWIP being illuminated with incident radiation at 9.0 μm wavelength, since 0.3 μm is about 1/10 the wavelength in GaAs. However, a high-conductivity metal such as gold may have a skin depth of ~100 Å, requiring a grid spacing of ~10 Å, which would result in far too many grid cells to calculate in any reasonable time. Instead of this "brute-force" approach, we used the "synthetic conductivity" method [20], which employs a derived conductivity value that, when used in the FDTD difference equations, yields the correct surface impedance. Therefore, the fields outside the metal are nearly correct, even though the fields inside may not be.

Table 1 shows the material properties used, unless otherwise noted. The values are based on published values as well as fits to experimental data. The QW stack is composed of many alternating layers of GaAs and AlGaAs, for example; however, since the layer thicknesses are much less than a wavelength, the stack was modeled as a homogeneous material with spatially averaged properties. The permittivity of the QW stack was deduced from published data for GaAs and AlAs and from the peak wavelength of earlier grating-coupled QWIPs. The conductivity perpendicular to the QW stack was deduced from calibrated absorption measurements on specially processed QWIP test bars [21]. These measurements indicated an absorption cross-section of $\sigma_0 \approx 1.5 \times 10^{-14}$ cm^2 per electron for typical GaAs/AlGaAs QWIP material grown at ARL, which corresponds to an absorption length of ~15 μm for a typical average doping of $n_{3D} \approx 4.4 \times 10^{16}$ cm^{-3} in the QW stack (e.g., $n_{3D} \approx 4 \times 10^{17}$ cm^{-3} doping in 60-Å wells separated by 440-Å undoped barriers). A value of 460 S/m was found to match these data, but a value of 1000 S/m was used in most of the calculations shown below to simulate the higher absorption achievable with coupled-well structures [22]. Although the frequency-dependent conductivity of the QW stack can be incorporated into the FDTD calculations, we used a constant conductivity for all results presented here so that the coupling efficiency could be seen over a broad spectral range.

The incident field on the pixel was a normally incident plane wave with a Gaussian-modulated sinusoidal temporal profile. The Gaussian modulation in the time domain corresponds to a Gaussian envelope of incident frequencies in the frequency domain. Since the FDTD method and all of our materials are linear, the different frequencies in the incident field propagate independently through the time stepping. Therefore, Fourier analysis on the time-dependent absorption

Table 1
Material properties used in FDTD calculations

Material	Parallel to QWs		Perpendicular to QWs	
	Permittivity	Conductivity (S/m)	Permittivity	Conductivity (S/m)
GaAs contact	9.92	0.0	9.92	0.0
QW stack	9.92	0.0	9.92	1000
Gold	1.0	1.53×10^{7}[a]	1.0	1.53×10^{7}[a]

[a] "Synthetic" conductivity for 0.05 μm cell (see text).

at each point in the QW stack yields the absorption and QE at all of the incident frequencies. In other words, we get a full spectrum of QE in roughly the same time that the steady-state method yields the value at a single wavelength.

We used a cell size of either 0.025 or 0.05 μm. These dimensions are equal to $\sim 1/120$ and $\sim 1/60$ wavelength in GaAs, respectively. They are much smaller than typically required for accuracy in FDTD, but were used to accurately describe the thin layers in the antenna structure. The results obtained using the two cell sizes were nearly equivalent.

We computed most of the results for a single unit cell of the microstrip antenna with periodic boundary conditions (BCs) imposed to simulate an infinitely large pixel. We obtained the finite-pixel results by modeling an entire pixel, using periodic BCs to simulate the presence of an infinite FPA around the modeled pixel.

3. Results

Fig. 3 shows the calculated spectral QE for several antenna sizes and periods. The slab consisted of a 0.2-μm-thick QW stack between two 0.1-μm-thick GaAs contact layers. Note that the peak wavelength is primarily a function of the antenna size, as expected for antenna coupling, and only varies weakly with the antenna period. This contrasts with grating coupling, in which the peak wavelength is proportional to the period. The shift in peak wavelength in Fig. 3 is actually in the opposite direction to that expected from grating coupling.

Fig. 4 shows the variation in spectral QE with the thickness of the QW layer. Note that as the thickness increases, the spectrum becomes broader and shifts to longer wavelength. This can be understood by noting the fields in Fig. 2b. As the thickness increases, the region of curving fields at

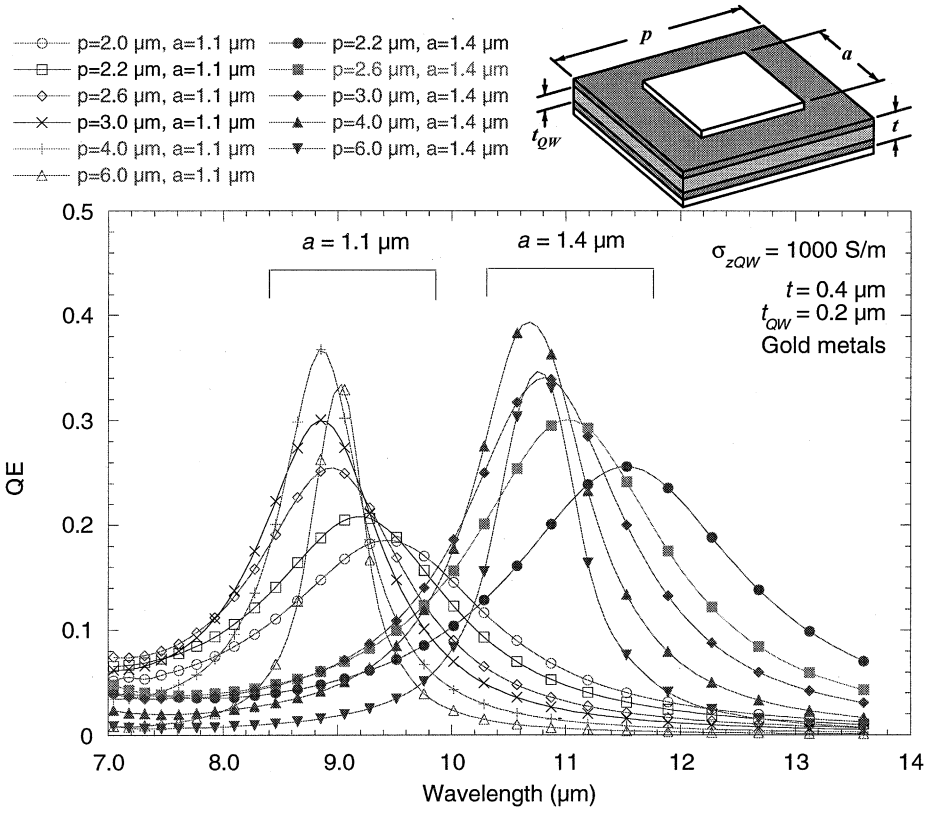

Fig. 3. Spectral QE versus antenna size a and period p.

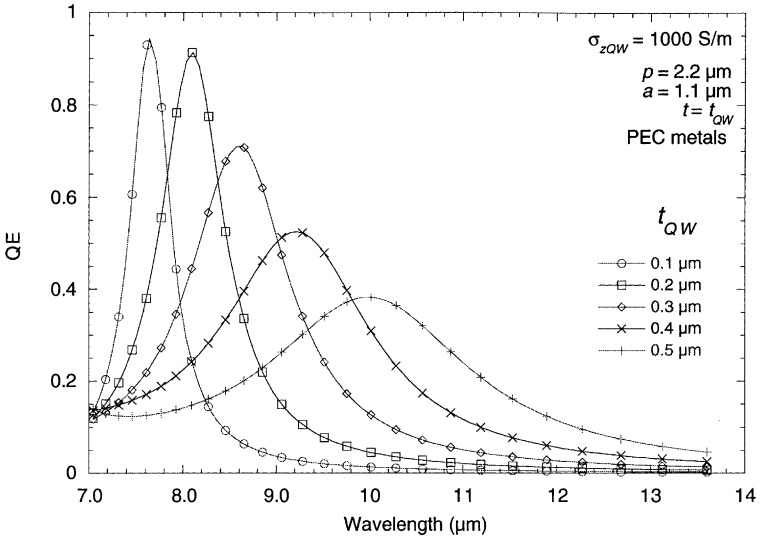

Fig. 4. Spectral QE versus QW-layer thickness.

the ends of the pixel broaden and extend outward, so that the effective length of the antenna is increased. A QW-layer thickness of 0.1–0.2 μm (total thickness of 0.3–0.4 μm) yields a spectral width that matches the natural spectral absorption width of typical QW material, and therefore would yield the largest spectrally integrated response.

Fig. 5 shows the variation in spectral QE with the absorption strength of the QW material, with use of perfect electrical conductor (PEC) for the antenna and ground plane. Note that the QE approaches 100% for very large values of σ_{zQW}, i.e., for very high QW absorption strength. The higher values of σ_{zQW} are almost certainly not achievable in real QW material, but demonstrate the ultimate limit of the microstrip structure.

The structures modeled in Fig. 3 through Fig. 5 have a QW stack sandwiched between two 0.1-μm-thick GaAs contact layers, so the average absorption strength in the absorbing region under the antenna is less than that of the QW material itself. Therefore, to achieve the highest possible QE, the contact layers should be made as thin as possible. Fig. 6 shows the spectral absorption in the QW region, antenna, and ground plane for a structure in which the contact layer thicknesses were reduced to 0.05 μm. Note that although the total absorption is very large, more than half the

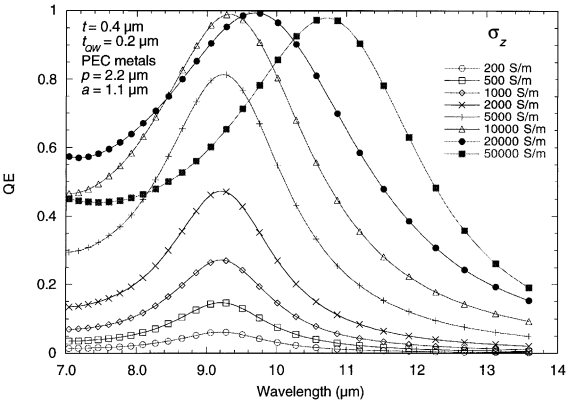

Fig. 5. Spectral QE as a function of QW absorption strength for a design with 0.2-μm-thick QW stack and 0.1-μm-thick GaAs contact layers.

energy is absorbed in gold layers. Fig. 7 shows the spatial distribution of the absorption at the peak wavelength of 8.90 μm. The QW absorption is concentrated near the edges of the pixel, while the metal absorption is concentrated near the center. This is consistent with the field patterns shown in Fig. 2b. The E_z component of the light propagating in from the edges of the pixel cancels at the center of the pixel, but constructively interferes near the edges. On the other hand, H constructively interferes near the center so that the total H,

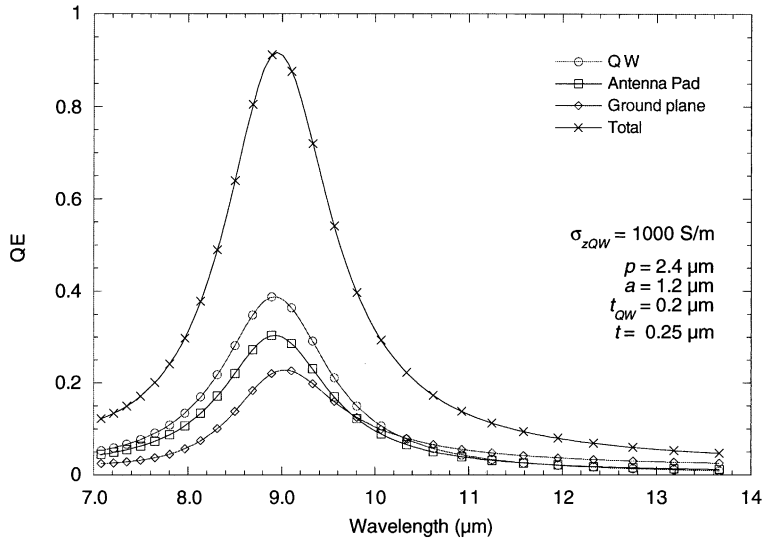

Fig. 6. Spectral absorption in QW material, gold antenna, and ground plane layers.

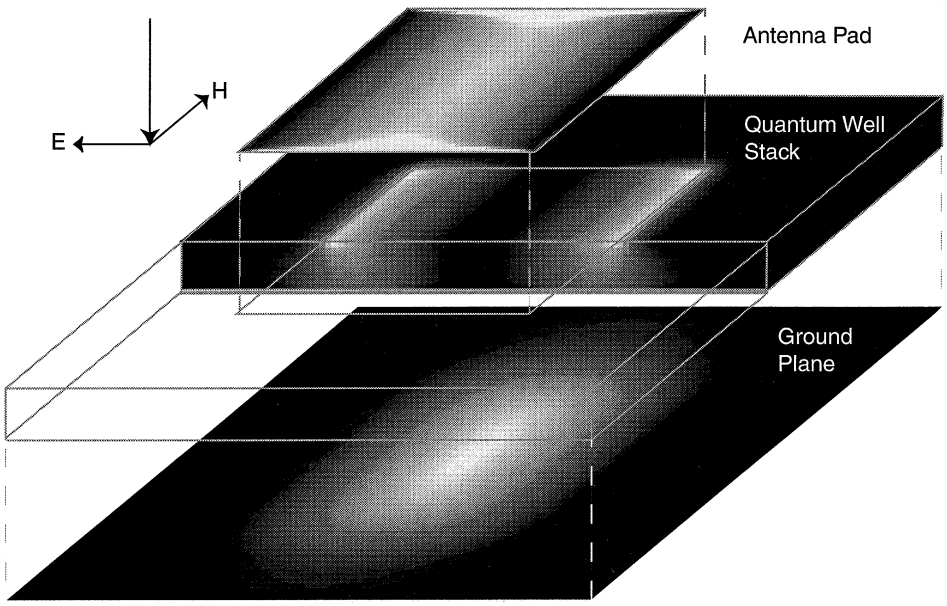

Fig. 7. Absorption in microstrip antenna corresponding to absorption spectra in Fig. 6.

and the corresponding surface currents in the metal, are maximum there. In addition, energy is absorbed along the sides of the antenna pad where the incident field excites currents parallel to the edge.

Finally, Fig. 8 shows a comparison of the spectral QE for an infinite pixel versus a 22-μm pixel on 24-μm centers. The result for the finite pixel has almost the same shape as for the infinite pixel, and is only slightly lower. Since a

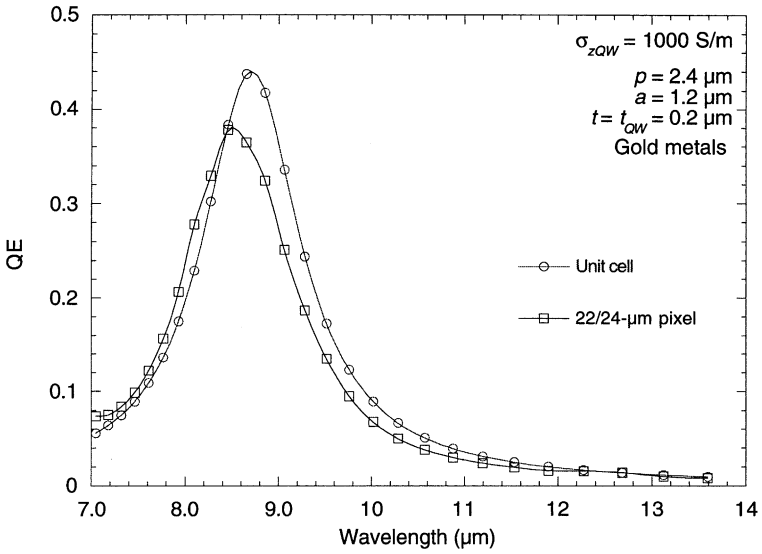

Fig. 8. Spectral QE of unit cell and 22-μm pixel on 24-μm period.

16% reduction is expected from the fill factor, this result shows excellent scaling and is consistent with coupling by localized fields under the antenna rather than by extended modes.

Since Fig. 7 shows that the metal absorption occurs primarily near the center of the pixel, we modeled a structure in which the solid antenna was replaced by an antenna with a square hole in its center. The hope was that light coming from the edges towards the center would remain trapped within the QW stack by total internal reflection, but without the large metal absorption, so that a higher QE would result. However, Fig. 9 shows that, as the hole is made larger, the peak QE actually decreases and shifts to longer wavelength.

4. Discussion

The calculated QE with the microstrip antenna is comparable to that of grating-couple QWIPs. However, the QE is achieved in a much thinner structure, so the photoconductive gain will be much larger. For example, a typical QWIP uses ~40 wells, has a QW stack that is ~2.3 μm thick, and a gain of ~0.2. A similar microstrip-antenna-coupled QWIP that is 0.3 μm thick would have ~5 wells and a gain of ~1.5. When operated at higher temperatures, where dark current noise dominates, the ~7 times higher gain would increase the normalized detectivity D^* by a factor of about 2.8 over a grating-coupled QWIP with the same QE. At lower temperatures where the operation is background limited, there would be no improvement in D^*, but there would be an increase in both signal and noise, which may be useful to overcome readout noise.

The microstrip antenna structure may also provide a good way to couple to single-QW structures that are sometimes grown to investigate the properties of an isolated well or because strain precludes the growth of multiple wells.

The maximum QE that can be achieved with reasonable values for the QW absorption strength is around 40–50%, and is limited by resistive losses in the antenna and ground plane. There are fundamental reasons why resistive loss is a more significant problem in antennas operated at infrared, compared to microwave, frequencies. First, the skin depth is smaller at infrared frequencies, so the surface conductance is also smaller, and the resistive loss is therefore larger per area of metal. For example, the skin depth of gold having an assumed bulk conductivity of 4.6×10^7 S/m is 0.43 μm at a

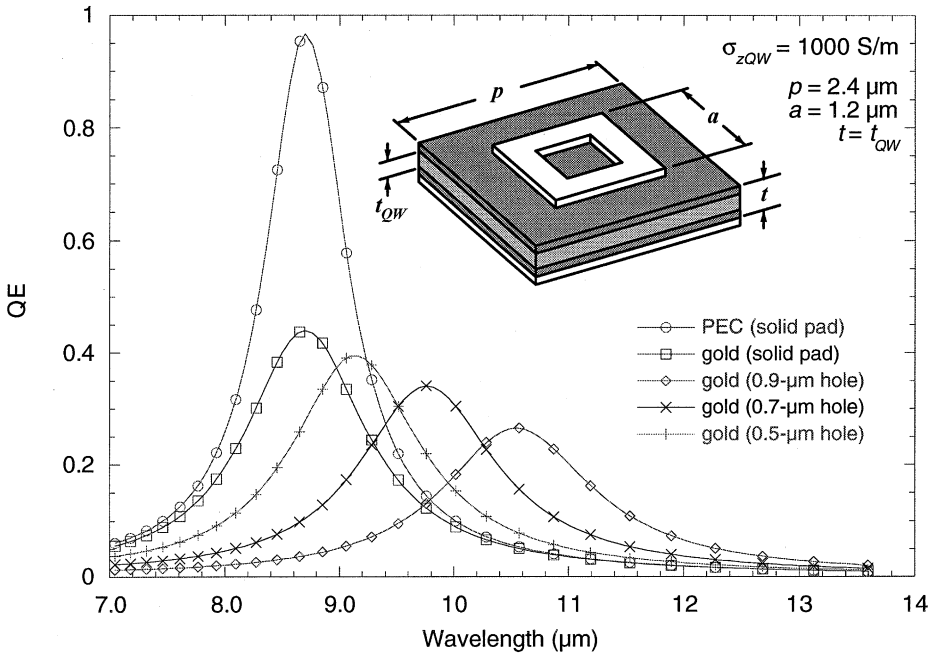

Fig. 9. Spectral QE for antenna with hole versus solid antenna.

wavelength of 1 cm, but only 0.014 μm at a wavelength of 10 μm. The corresponding surface conductances are 19.7 and 0.62 S, respectively. Second, as the dimensions of the overall structure shrink with the wavelength, the loss in the metals tends to decrease proportional to the square of the linear dimension while the bulk absorption tends to decrease proportional to the cube. The net effect is that resistive loss is often a major effect in infrared antenna or grating structures, even when gold is used.

Resistive loss is also one of the problems with implementing the transmission-line readout shown in Fig. 1. Such structures would be useful for polarization-sensitive or two-colour imaging. However, our results indicate that the energy from the antenna would be rapidly dissipated in the metal of the transmission line. In addition, a transmission line whose impedance matches the antenna requires a very narrow line width of less than 0.1 μm, which could not be fabricated with current techniques.

In summary, we have shown that the microstrip antenna should provide good coupling for QWIPs, and that QE of 20–40% should be possible, even with thin (0.3-μm) QW stacks. These thinner structures should yield higher D^* than thick structures with the same QE in dark-current-limited detectors. The QE is limited by resistive loss in the metal layers, even with gold, and by the relatively long absorption lengths that exist in current QW material. Current absorption lengths of around 15 μm are comparable to the width of typical pixels, so high QE is only possible in resonant coupling structures that achieve multiple passes, but at the cost of narrow spectral bandwidth.

References

[1] G. Hasnain, B.F. Levine, C.G. Bethea, R.A. Logan, J. Walker, R.J. Malik, Appl. Phys. Lett 54 (1989) 2515.
[2] J.Y. Andersson, L. Lundqvist, Appl. Phys. Lett. 59 (1991) 857.
[3] J.Y. Andersson, L. Lundqvist, Z.F. Paska, Appl. Phys. Lett 58 (1991) 2264.
[4] J.Y. Andersson, L. Lundqvist, J. Appl. Phys. 71 (1992) 3600–3610.

[5] G. Sarusi, B.F. Levine, S.J. Pearton, K.M.S. Bandara, R.E. Leibenguth, Appl. Phys. Lett 64 (1994) 960.
[6] S.I. Borenstain, U. Arad, I. Lyubina, A. Segal, Y. Warschawer, Appl. Phys. Lett. 75 (1999) 2659–2661.
[7] W.J. Li, B.D. McCombe, J. Appl. Phys. 71 (1992) 1038.
[8] S.D. Gunapala, J.K. Liu, M. Sundaram, J.S. Park, C.A. Shott, T. Hoelter, T.L. Lin, S.T. Massie, P.D. Maker, R.E. Muller, G. Sarusi, in: Proceedings of the 188th Meeting of the Electrochemical Society Chicago, IL, 1995.
[9] T.R. Schimert, S.L. Barnes, A.J. Brouns, F.C. Case, P. Mitra, L.T. Claiborne, Appl. Phys. Lett. 68 (1996) 2846.
[10] C.J. Chen, K.K. Choi, M.Z. Tidrow, D.C. Tsui, Appl. Phys. Lett. 68 (1996) 1446.
[11] I. Wilke, W. Hermann, F.K. Kneubühl, Appl. Phys. B 58 (1994) 87–95.
[12] N. Chong, H. Ahmed, Appl. Phys. Lett. 71 (1997) 1607–1609.
[13] C. Fumeaux, W. Hermann, F.K. Kneueühl, H. Rothuizen, Infrared Phys. Technol. 39 (1998) 123–183.
[14] E.N. Grossman, J.E. Sauvageau, D.G. McDonald, Appl. Phys. Lett. 59 (1991) 3225–3227.
[15] W.A. Beck, M.S. Mirotznik, T.S. Faska, in: Proceedings of the Fifth International Symposium on Long Wavelength Infrared Detectors and Applications: Physics and Applications, Paris, 1997.
[16] R.E. Munson, in: R.C. Johnson, H. Jasik (Eds.), Antenna Engineering Handbook, 2nd ed., McGraw-Hill, New York, 1984.
[17] I. Codreanu, G.D. Boreman, http://www.creol.ucf.edu/~iulian/research.dir/experimental.html, 1999.
[18] K.S. Kunz, R.J. Luebbers, The Finite Difference Time Domain Method in Electromagnetics, CRC Press, Boca Raton, 1993.
[19] A. Taflove, Computational Electrodynamics: The Finite-Difference Time-Domain Method, Artech House, Boston, 1995.
[20] K. Chamberlin, L. Gordon, IEEE Trans. Electromag. Compat. 37 (1995) 210.
[21] J.W. Little, unpublished results, 1999.
[22] S.W. Kennerly, D.W. Beekman, J.W. Little, A.C. Goldberg, R.P. Leavitt, in: Proceedings of the IRIS Speciality Group on Detectors, Boulder, CO, 1998.